Becoming a Member

Membership of The Physiological Society offers you access to the largest network of physiologists in Europe. Our aim is to support physiology to ensure it remains at the forefront of biological and medical research. Whether you are established in your career or starting out in the field of physiology, we have a membership option for you. Members benefit from reduced registration rates for our events, free online access to The Physiological Society's journals – *The Journal of Physiology* and *Experimental Physiology* – and travel grants to attend scientific meetings. Be part of our growing membership of over 3000 and access unrivalled networking opportunities to develop and further your career in physiology.

The Society's meetings enable you to keep up-to-date with research developments, present your own work and forge new collaborations with other Members. Our annual Main Meeting is now one of the biggest international physiological meetings in the calendar, attracting over 1000 scientists from around the world.

Networks

We have more than 3000 Members in over 60 countries

History

The Physiological Society was founded in 1876

Join now to:

Access science

New research from across the discipline is presented at our scientific meetings

Free online access to *The Journal of Physiology* and *Experimental Physiology*

Access networks

The opportunity to attend Society events at a discounted rate

Our Members' website provides online networking opportunities and links to Member-specific initiatives

Support your career

Grant funding for travel, attendance at scientific meetings and outreach projects

Training in specialist techniques

For more information, or to discuss membership options, please visit www.physoc.org or call 020 7269 5728

www.physoc.org

The Physiological Society

aptara | TJP | tjp6059 | Dispatch: February 7, 2014 | CE: N / A
Journal | MSP No. | No. of pages: 14 | PE: Richard

The Journal of Physiology

Hypermuscular mice with mutation in the Myostatin gene display altered calcium signalling

Dóra Bodnár[1], Nikolett Geyer[1], Olga Ruzsnavszky[1], Tamás Oláh[1], Bence Hegyi[1], Mónika Sztretye[1], János Fodor[1], Beatrix Dienes[1], Ágnes Balogh[2], Zoltán Papp[2], László Szabó[3], Géza Müller[1], László Csernoch[1] and Péter Szentesi[1]

[1]*Department of Physiology, Medical and Health Science Centre, University of Debrecen, Debrecen, Hungary*
[2]*Department of Cardiology, Medical and Health Science Centre, University of Debrecen, Debrecen, Hungary*
[3]*Department of Electrical Engineering, Sapientia Hungarian University of Transylvania, Târgu Mureș, Romania*

Key points

- Hypermuscularity associated with naturally occurring mutations in the myostatin gene as found in *Compact* mice results in increased muscle mass but reduced specific force.
- The calcium sensitivity of the contractile apparatus as assessed on chemically skinned skeletal muscle fibres under isometric conditions is not altered in these animals.
- While the resting calcium concentration remains unaffected, depolarization-evoked increases in intracellular calcium concentration are suppressed.
- Spontaneous calcium release events from sarcoplasmic reticulum are also decreased in frequency, amplitude and spatial spread.
- Our results suggest that mutations in the myostatin gene are accompanied by alterations in excitation contraction coupling, which manifest as a reduction in sarcoplasmic calcium release.

Abstract Myostatin, a member of the transforming growth factor β family, is a potent negative regulator of skeletal muscle growth, as myostatin-deficient mice show a great increase in muscle mass. Yet the physical performance of these animals is reduced. As an explanation for this, alterations in the steps in excitation–contraction coupling were hypothesized and tested for in mice with the 12 bp deletion in the propeptide region of the myostatin precursor ($Mstn^{Cmpt\text{-}dl1Abc}$ or *Cmpt*). In voluntary wheel running, control C57/BL6 mice performed better than the mutant animals in both maximal speed and total distance covered. Despite the previously described lower specific force of *Cmpt* animals, the p_{Ca}–force relationship, determined on chemically permeabilized fibre segments, did not show any significant difference between the two mouse strains. While resting intracellular Ca^{2+} concentration ($[Ca^{2+}]_i$) measured on single intact flexor digitorum brevis (FDB) muscle fibres using Fura-2 AM was similar to control (72.0 ± 1.7 *vs.* 78.1 ± 2.9 nM, $n = 38$ and 45), the amplitude of KCl-evoked calcium transients was smaller (360 ± 49 *vs.* 222 ± 45 nM, $n = 22$) in the mutant strain. Similar results were obtained using tetanic stimulation and Rhod-2 AM, which gave calcium transients that were smaller (2.42 ± 0.11 *vs.* 2.06 ± 0.10 $\Delta F/F_0$, $n = 14$ and 13, respectively) on *Cmpt* mice. Sarcoplasmic reticulum (SR) calcium release flux calculated from these transients showed a reduced peak (23.7 ± 3.0 *vs.* 15.8 ± 2.1 mM s^{-1}) and steady level (5.7 ± 0.7 *vs.* 3.7 ± 0.5 mM s^{-1}) with no change in the peak-to-steady ratio. The amplitude and spatial spread of calcium release events detected on permeabilized FDB fibres were also significantly smaller in mutant mice. These results suggest that reduced SR calcium release underlies the reduced muscle force in *Cmpt* animals.

DOI: 10.1113/jphysiol.2013.261958

(Received 5 September 2013; accepted after revision 16 January 2014; first published online 20 January 2014)
Corresponding author P. Szentesi: Department of Physiology, Faculty of Medicine, Medical and Health Science Centre, University of Debrecen, PO Box 22, H-4012 Debrecen, Hungary. Email: szentesi.peter@med.unideb.hu

Abbreviations ECC, excitation–contraction coupling; EDL, extensor digitorum longus; FDB, flexor digitorum brevis; FWHM, full width at half maximum; RyR, ryanodine receptor; SR, sarcoplasmic reticulum; T-tubular, transverse-tubular

Introduction

Myostatin – originally named growth and differentiation factor-8 (GDF-8) – a member of the transforming growth factor β (TGF-β) superfamily, has emerged as a potent negative regulator of skeletal muscle growth (McPherron *et al.* 1997). It plays a key role in skeletal muscle homeostasis and has been well described since its discovery. During embryogenesis, myostatin is exclusively expressed in skeletal muscle to control the differentiation and proliferation of myoblasts (Langley *et al.* 2002). It mediates the cell signalling cascade through activin receptors in the muscle, which interfere with the activity and expression of myoblast determination protein (MyoD; Langley *et al.* 2002). Recently, myostatin has also been shown to inhibit Akt, a kinase that regulates muscle growth (Bodine *et al.* 2001; Lai *et al.* 2004), in part through the activation of protein synthesis (e.g. Elkina *et al.* 2011).

Myostatin was first identified when null-mutant knock-out mice exhibited a huge increase in skeletal muscle mass due to hypertrophy and hyperplasia (McPherron *et al.* 1997). Mutations causing hypermuscularity in the double-muscled Belgian Blue and Piedmontese cattle breeds were described in the myostatin gene (Kambadur *et al.* 1997). Similarly, whippet dogs with excessive muscle growth were found to have a heterozygous naturally occurring mutation (Mosher *et al.* 2007).

Hypermuscular mice were also found by several groups in selection studies examining the genetic basis of protein accretion (Varga *et al.* 1997; Bünger *et al.* 2001). These include the so-called 'Compact' mice (Varga *et al.* 1997), in which sequencing of the myostatin gene revealed a 12 bp deletion – and thus the name $Mstn^{Cmpt\text{-}dl1Abc}$ (Szabo *et al.* 1998) – in the propeptide region of the myostatin precursor. In homozygous *Cmpt*/*Cmpt* mutants, mature myostatin is active (Szabó *et al.* 1998), enabling genes modifying the expression of myostatin or modulating downstream signalling to have a significant influence on the hypermuscular phenotype (Varga *et al.* 2003).

Amthor *et al.* (2007) showed that despite the larger muscle mass relative to age-matched wild-types, there was no increase in maximal tetanic force generation, but rather that when expressed as a function of muscle size (specific force) extensor digitorum longus (EDL) muscles of myostatin knock-out ($Mstn^{-/-}$) and *Cmpt* mice were weaker than wild-type muscles. In addition, muscles from $Mstn^{-/-}$ animals had a marked increase in the number of type IIb fibres as compared to wild-type controls. They suggested that with myostatin deficiency, decreased force production is accompanied by a loss of oxidative characteristics of skeletal muscle.

On the other hand, while alterations in fibre type and oxidative characteristics of the muscles in *Cmpt* mice could explain a reduction in overall endurance, they fail to explain why specific force is decreased in these animals. Therefore, modifications in one or more of the events leading to shortening – i.e. in excitation–contraction coupling (ECC) – could be the underlying reason for the alterations in muscle force of *Cmpt* mice. Nevertheless, the steps in ECC have not yet been investigated in these animals.

In skeletal muscle ECC begins when depolarization of the transverse (T-)tubular membrane initiates the release of calcium from its intracellular store, the sarcoplasmic reticulum (SR), via specialized Ca^{2+} release channels known as ryanodine receptors (RyR; e.g. Franzini & Protasi, 1997). RyR activation is achieved by the depolarization-evoked conformational change of the dihydropyridine receptors (DHPRs) localized in the T-tubular membrane (e.g. Rios & Pizarro, 1991; Lamb, 2002). Calcium ions then bind to the regulatory sites on troponin-C to initiate a conformational change, which in turn enables the binding of myosin to actin and, ultimately, results in muscle contraction.

To understand the apparent discrepancy between increased muscle mass and reduced specific force reported in the literature for *Cmpt* mice, we hypothesized that ECC is also modified in these animals. To this end, we give an in-depth investigation of muscle function by comparing the physical endurance of control and *Cmpt* mutant mice as well as changes of ECC. For the latter, intracellular calcium concentration measurements were conducted using electrical stimulation or prolonged depolarization of enzymatically isolated fibres loaded with fluorescent calcium indicators while the contractile activation was studied on chemically skinned fibre segments. We demonstrate that reduced SR Ca^{2+} release underlies the suppression of specific force. Part of this work was presented to the European Muscle Society (Jenes *et al.* 2012).

Methods

Animal care

Animal experiments conformed to the guidelines of the European Community (86/609/EEC). The experimental protocol was approved by the institutional Animal Care Committee of the University of Debrecen (22/2011/DE MAB). The mice were housed in plastic cages with mesh covers, and fed with pelleted mouse chow and water *ad libitum*. Room illumination was an automated cycle of 12 h light and 12 h dark, and room temperature was maintained within the range 22–25°C. When necessary mice were killed by cervical dislocation.

Mating and genotyping of *Cmpt* mice

The *Cmpt* mice (see Supplementary Fig. S1*A* top, S1*B*) originated from G.M.'s lab (Varga *et al.* 2003). To monitor the *Cmpt* mutation, heterozygous mice were obtained by mating wild-type C57BL/6 ($Mstn^{+/+}$; control; Fig. S1*A* bottom, S1*C*) and *Cmpt* mice. Tail-tip biopsy was performed for genotyping (see Fig. S2).

In vivo experiments

Voluntary activity wheel measurement. Twelve- to 16-week-old *Cmpt* ($n = 8$) and C57BL/6 ($n = 8$) mice were singly housed in a cage with a mouse running wheel (Campden Instruments Ltd, Loughborough, UK). Wheels were interfaced to a computer and revolutions were recorded at 20 min intervals, continuously for 14 days. The average and maximal speed, and the distance and duration of running were calculated for individual mice and then averaged by strains.

Forepaw grip test. Twelve- to 16-week-old *Cmpt* ($n = 5$) and C57BL/6 ($n = 11$) mice were held perpendicular to the bar connected to a capacitive force transducer, so that they did not reach at an angle during the trials. The hind limbs were not allowed to touch any surfaces. When the unrestrained forepaw was brought into contact with the bar of the grip test meter, the animals reliably grasped the bar, and the animal was then gently pulled away from the device. The grip test meter then measured the maximal force before the animal released the bar. We allowed the mouse to grip the bar fully. Force responses were digitized at 2 kHz and stored via an online connected computer.

In vitro experiments

Isolation of single skeletal muscle fibres. Experiments were carried out on skeletal muscle fibres from the flexor digitorum brevis (FDB), EDL and soleus muscles of the mice. Single muscle fibres were enzymatically dissociated in calcium-free modified Tyrode's solution (in mM: 137 NaCl, 5.4 KCl, 0.5 $MgCl_2$, 11.8 Hepes, pH 7.4) containing 0.2% Type I collagenase (Sigma, St Louis, MO, USA) at 37°C for 50–55 min (Csernoch *et al.* 2008).

To release single fibres muscles were triturated gently in modified Tyrode's solution supplemented with 1.8 mM $CaCl_2$. The fibres were then mounted on laminin-coated cover slip floors of culture dishes and kept at 4°C until use.

Resting membrane potential measurement

FDB muscle fibres were superfused with oxygenized Tyrode's solution (in mM: 137 NaCl, 5.4 KCl, 0.5 $MgCl_2$, 1.8 $CaCl_2$, 11.8 Hepes-NaOH, 1 g l^{-1} glucose, pH 7.4) at room temperature (22°C). Only cells with an intact surface membrane and clear cross striations were used. Membrane potentials were recorded using 3 M KCl filled sharp glass microelectrodes having tip resistances between 30 and 40 MΩ. The electrodes were connected to the input of a Multiclamp-700A amplifier (Axon Instruments, Foster City, CA, USA) under current clamp conditions. Membrane potentials were digitized at 100 kHz using a Digidata 1322 A/D card (Axon Instruments) under software control (pClamp 9.2, Axon Instruments) and stored for later analysis.

Ca^{2+} sensitivity of the contractile proteins

Ca^{2+}-dependent active isometric force and its Ca^{2+} sensitivity, and Ca^{2+}-independent passive force of permeabilized EDL and soleus muscle fibres were determined by a mechanical measuring system at 15°C as previously described (Papp *et al.* 2002; for additional details see Supplementary Material). Briefly, Ca^{2+} contractures were evoked by transferring the fibres from Ca^{2+}-free relaxing solution (in mM: 37.34 KCl, 10 BES, 6.24 $MgCl_2$, 7 EGTA, 6.99 Na_2ATP and 15 sodium creatinin-phosphate, pH 7.2) to activating solutions (relaxing solution supplemented with Ca) of gradually increasing [Ca^{2+}]. During single Ca^{2+} contractures, when the force reached the maximal value, a quick release–re-stretch manoeuvre was performed in the activating solution. As a result of this intervention, the force dropped from peak level to zero, allowing determination of the total force level (F_{total}), and then started to redevelop. Force redevelopment was fitted to a single exponential function to estimate the rate constant of force redevelopment (k_{tr}). The fibre was then returned to the relaxing solution, where a shortening to 80% of the original preparation length was performed to assess the passive force level ($F_{passive}$). The active isometric force (F_{active}) was calculated by subtracting $F_{passive}$ from F_{total}. F_{active} and $F_{passive}$ were normalized for

the fibre cross-sectional area calculated from the width and height of the fibres. Isometric force values were normalized for the maximal Ca^{2+}-activated active force, and Ca^{2+}–force relationships were plotted to determine the Ca^{2+} sensitivity of isometric force production.

The relationship between force and p_{Ca} was fitted with a modified Hill equation:

$$F_{Ca} = F_{max}([Ca^{2+}]^{nH}/(pCa_{50}^{nH} + [Ca^{2+}]^{nH})) + F_{min}, \quad (1)$$

where F_{Ca} is the steady-state force, F_{max} is the steady isometric force at saturating Ca^{2+} concentration ($p_{Ca} = 4.75$), the Hill coefficient (nH) is a measure of the steepness of the relationship, p_{Ca50} is the midpoint of the relationship and F_{min} is defined as the isometric force recorded at $p_{Ca} = 9$.

Whole-cell intracellular Ca^{2+} concentration measurement

Changes in intracellular Ca^{2+} concentration ($[Ca^{2+}]_i$) were monitored using Fura-2 as described previously (Fodor *et al.* 2008; for additional details see Supplementary Material). Briefly, isolated FDB fibres were mounted on laminin-coated cover slips and loaded with 5 μM Fura-2 AM for 60 min. Ca^{2+} transients were evoked by KCl depolarization. $[Ca^{2+}]_i$ was calculated from the ratio of measured fluorescence intensities (F_{340}/F_{380}) using an *in vivo* calibration as described in our earlier report (Fodor *et al.* 2008).

Detection of the changes in $[Ca^{2+}]_i$ using confocal microscopy

Individual action potentials were evoked by applying supra-threshold 2 ms square pulses (S88 Stimulator, Grass Technologies, Warwick, RI, USA) through a pair of platinum electrodes placed close to the fibre. Tetanic depolarizations were initiated using trains of supra-threshold 2 ms square pulses with a frequency of 100 Hz within the train. Each train lasted for 500 ms. Depolarization-evoked calcium transients were measured at 22°C using a confocal laser scanning microscope system (Zeiss 5 Live, Oberkochen, Germany) after loading the fibres with 20 μM Rhod-2 AM for 15 min at room temperature. Line-scan images (512 pixels per line) were used to monitor the fluorescence intensity changes at 1 ms per line and using a 40× water immersion objective. Rhod-2 was excited with a helium–neon ion laser at 543 nm, and emission was detected with a 550 nm long pass filter. To obtain the time course of Rhod-2 fluorescence change (F_{rhod}), corresponding data points (usually 10–15) in the line-scan images were averaged in the spatial domain. Resting fluorescence was determined as the average fluorescence before the depolarization. Changes in $[Ca^{2+}]_i$ were then calculated using the formula

$$[Ca^{2+}]_i = Kd_{rhod} \cdot (F_{rhod} - F_{rhod,min})/(F_{rhod,max} - F_{rhod}) \quad (2)$$

where $F_{rhod,max}$ and $F_{rhod,min}$ were determined in our laboratory, while other parameters ($k_{off,rhod}$ and $k_{on,rhod}$, backward and forward rate constants for the calcium-dye reaction, respectively, with $Kd_{rhod} = k_{off,rhod}/k_{on,rhod}$) for Rhod-2 were taken from Escobar *et al.* (1997).

Table 1. Grip-strength test data

	Control ($n = 11$)	*Cmpt* ($n = 5$)[#]
Body weight (g)	20.7 ± 0.7	56.0 ± 3.3***
Absolute force (mN)	71.1 ± 1.4	126.7 ± 4.0***
Force normalized to body weight (mN g^{-1})	3.48 ± 0.07	2.36 ± 0.09***

***Significant difference at $P < 0.001$ as compared to control.
[#]Numbers in parentheses denote the number of animals.

Table 2. Distance and speed in voluntary wheel running

	Control ($n = 8$)	*Cmpt* ($n = 8$)[#]
Distance (m day^{-1})	7145 ± 553	3387 ± 283**
Average speed (m min^{-1})	13.3 ± 1.0	9.6 ± 0.8**
Maximal speed (m min^{-1})	23.1 ± 1.0	18.6 ± 1.0**
Duration (min day^{-1})	544 ± 31	356 ± 25**

**Significant difference at $P < 0.01$ as compared to control.
[#]Numbers in parentheses denote the number of animals.

Detection of calcium release events

After enzymatic dissociation, FDB fibres were permeabilized using 0.01% saponin for a few seconds. Spontaneous calcium release events were visualized by 50 μM Fluo-3 using a confocal laser scanning microscope (Zeiss 5 META, Oberkochen, Germany) at 22°C (as described by Lukacs *et al.* 2008; for additional details see Supplementary Material).

Images containing spontaneous calcium release events were analysed using an automatic event detection program (Szentesi *et al.* 2004; Szabo *et al.* 2010), which calculated the amplitude ($\Delta F/F_0$), full width at half maximum (FWHM), rise time and duration of the identified events.

Table 3. Calcium sensitivity of isometric force

	Control		*Cmpt*	
	EDL ($n = 8$)	Soleus ($n = 8$)	EDL ($n = 7$)	Soleus ($n = 8$)[#]
Cross section (μm^2)	1887 ± 343	1714 ± 235	2602 ± 380	3303 ± 386**
T_{active} (kN m^{-2})	26.14 ± 5.06	26.87 ± 3.98	25.25 ± 4.01	21.89 ± 2.18
$T_{passive}$ (kN m^{-2})	2.24 ± 0.58	2.07 ± 0.48	2.15 ± 0.47	2.86 ± 0.37
k_{tr} (s^{-1})	3.43 ± 0.39	1.98 ± 0.21	6.15 ± 0.65**	1.84 ± 0.40
p_{Ca50}	5.73 ± 0.02	5.73 ± 0.04	5.77 ± 0.03	5.78 ± 0.05
nH	3.21 ± 0.19	3.12 ± 0.29	3.15 ± 0.16	2.75 ± 0.20

**Significant difference at $P < 0.01$ as compared to control.
[#]Numbers in parentheses denote the number of fibres from four control and four *Cmpt* animals.

Calculation of calcium release from the SR

The Ca^{2+} release flux (R_{rel}) was defined as the sum of Ca^{2+} fluxes entering the myoplasmic space and that transported back into the calcium storage organelle:

$$R_{rel} = d[Ca]_T/dt = d(Ca_{total} + Ca_{transp})/dt, \quad (3)$$

where Ca_{total} is the total Ca^{2+} in the myoplasm, and Ca_{transp} is the amount of Ca^{2+} transported by the removal processes. Ca_{total} was estimated as the sum of free Ca^{2+} (Ca_{free}) and the amount of Ca^{2+} bound to intracellular binding sites such as dye (Ca_{dye}), troponin-C (Ca_{tropC}), parvalbumin (Ca_{parv}) and pump (Ca_{pump}):

$$Ca_{total} = Ca_{free} + (Ca_{dye} + Ca_{tropC} + Ca_{parv} + Ca_{pump}), \quad (4)$$

In eqn (3) Ca_{transp} is the calcium quantity carried by Ca^{2+} removal mechanisms (pumps), which was considered proportional to the relative saturation of the pumps ($[Ca_{pump}]/[pump]$). The proportionality factor is the maximum speed of Ca^{2+} removal (PV_{max}):

$$Ca_{transp} = PV_{max} \cdot ([Ca_{pump}]/[pump]), \quad (5)$$

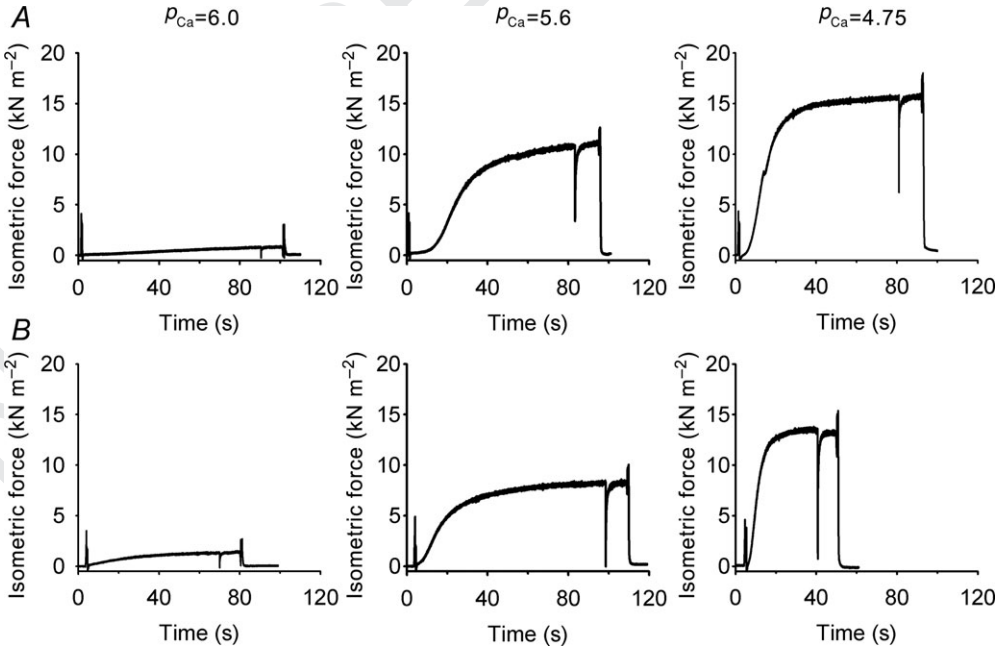

Figure 1. Time course of isometric force on skinned muscle fibres
Isometric force was measured on chemically skinned (0.5% Triton-X 100) fibre segments isolated from the EDL muscle of control (*A*) and of *Cmpt* (*B*) mice at three different calcium concentrations ($p_{Ca} = 6.0$, 5.6 and 4.75). Fibres were rapidly transferred from a relaxing solution ($p_{Ca} = 9$) to the test solutions and the time-course of force development was recorded. In all cases a rapid release and re-stretch manoeuvre was also performed. Experimental conditions: fibre cross section area 1764 and 2074 μm^2 in control and *Cmpt* mice, respectively; temperature 15°C.

Removal parameters were taken from the literature (Schuhmeier *et al.* 2003; Jacquemond 2012) and used as described in our earlier reports (Csernoch *et al.* 1990; Szappanos *et al.* 2004).

Chemicals and statistical analysis

Chemicals, unless otherwise stated, were purchased from Sigma and were of analytical grade. Pooled data were expressed as mean ± standard error of the mean (SEM). The differences between control and *Cmpt* animals were assessed using one-way analysis of variance (ANOVA) and all pair-wise multiple comparison procedures (Student–Newman–Keuls method). An *F*-test was used to test the significance and $P < 0.05$ was considered to indicate a statistically significant difference.

Results

In vivo experiments

Cmpt mice displayed great hypermuscularity and their weight was more than tice that of control animals (see Fig. S1, Table 1). To check the *in vivo* muscle performance of the adult animals, 12–16-week-old mice were used from both groups in grip tests. As expected, based on the increased muscle mass, *Cmpt* mice performed significantly better than the wild-type animals in these tests. That is, the maximal force that they could produce was significantly greater than that of control animals. However, after normalization to body weight – to compensate for the increased muscle mass – wild-type mice displayed significantly greater relative force as compared to the *Cmpt* animals (Table 1).

Experiments with the voluntary wheel gave similar results. Control mice performed significantly better given both the average and maximal speed and the total distance covered. In addition, they spent more time in the wheel than *Cmpt* mice (Table 2). Overall, these experiments clearly indicated that although *Cmpt* mice were larger and stronger, their strength was less than would be expected from the increase in muscle mass. To clarify the mechanisms underlying this, the steps in ECC were investigated in detail.

In vitro experiments

Resting membrane potential. To exclude the possibility that the electrical properties of the cell membrane were substantially altered, the resting membrane potential of FDB muscle fibres from four control and three *Cmpt* animals was determined. Although average resting membrane potential was slightly depolarized in *Cmpt* animals (-77.8 ± 0.2 mV, $n = 18$) as compared to control mice (-79.2 ± 0.3 mV, $n = 13$), we do not consider this difference to be physiologically relevant.

Calcium sensitivity of the contractile system. As the next step, the possible alterations in the contractile machinery were studied in both *Cmpt* and control mice. Force development during isometric contractions was measured in 31 fibre segments (segment length 80.7 ± 5.1 μm) dissected from soleus and EDL fibres of four wild-type and four *Cmpt* mice. Figure 1 displays six

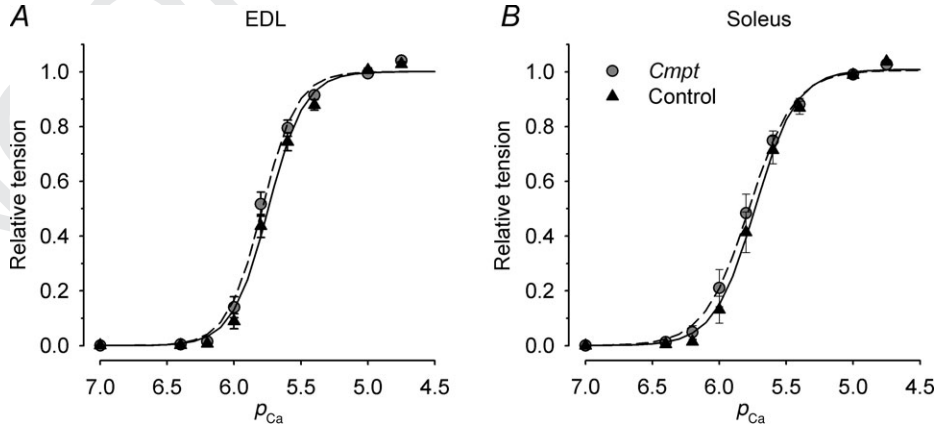

Figure 2. Calcium concentration dependence of isometric force
Maximal steady isometric force was determined for EDL (*A*) and soleus (*B*) muscles in control (black triangles) and in *Cmpt* mice (grey circles) at different calcium concentrations. These values were then normalized to those measured at $p_{Ca} = 4.75$, averaged over the individual fibres and plotted as a function of the calcium concentration of the activating solution. The lines indicate the Hill curves (eqn (1)) fitted to the data points (continuous line, control; dashed line, *Cmpt*). Parameters used to generate the fitted curves were: for EDL, nH = 3.21 and 3.32, $p_{Ca50} = 5.74$ and 5.79; for soleus, nH = 2.82 and 2.59, $p_{Ca50} = 5.73$ and 5.78 in control and *Cmpt*, respectively.

representative isometric contractions at low (p_{Ca} = 6.0), intermediate (p_{Ca} = 5.6) and saturating (p_{Ca} = 4.75) calcium concentrations. Table 3 presents the average maximal active and passive isometric tension (T_{active} and $T_{passive}$, respectively), which were obtained by normalizing the force values to the cross section of the fibre segments. There was no significant difference in these values between wild-type and *Cmpt* animals.

To gain further insight into the effects of the *Cmpt* mutation on force generation, the Ca^{2+} sensitivities of the isometric force on EDL and soleus muscles of control and *Cmpt* mice were compared (Fig. 2). After fitting eqn (1) to the data points, no significant difference was observed in p_{Ca50} or nH between the two groups of animals (Table 3). These results clearly suggest that the contractile machinery, including its calcium sensitivity, is not altered in the *Cmpt* strain.

Changes in $[Ca^{2+}]_i$ in *Cmpt* mice. Since the calcium sensitivity of the contractile proteins were similar in both groups of animals, the possible effects of the *Cmpt* mutation on calcium homeostasis was examined in isolated, single FDB skeletal muscle fibres of both types of mice. Twelve- to 16-week-old wild-type and *Cmpt* mice were used for functional experiments. Figure 3*A* presents calcium transients measured on these fibres evoked by depolarization using 120 mM KCl in the presence of a normal (1.8 mM) extracellular calcium concentration. The pooled data to confirm that the *Cmpt* mutation had little, if any, effects on the resting $[Ca^{2+}]_i$ (Fig. 3*B*), suggesting that the calcium leak from and the extrusion into the extracellular environment was unaffected under these conditions. On the other hand, depolarization-evoked calcium transients were almost 50% higher in control than in *Cmpt* fibres (Fig. 3*C*).

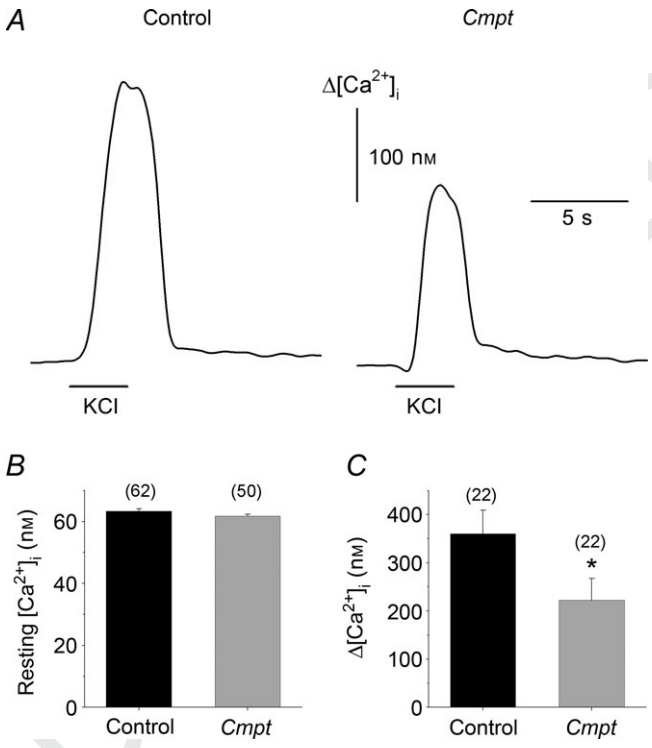

Figure 3. $[Ca^{2+}]_i$ at rest and during KCl-evoked depolarisations
A, depolarization-evoked changes in intracellular calcium concentration on intact fibres isolated from the FDB muscles of control (left) and of *Cmpt* (right) mice. Depolarization was achieved by the local perfusion of 120 mM KCl for 3 s as indicated by the horizontal lines below the transients. *B*, pooled data from three control and three *Cmpt* animals. Averaged values of resting $[Ca^{2+}]_i$ (*B*) and $\Delta[Ca^{2+}]_i$ (*C*). Numbers in parentheses are the number of fibres investigated. *Significant ($P < 0.05$) difference from control. Measurements were carried out at 22°C.

Action potential-evoked calcium transients in FDB fibres. Field stimulation-induced global calcium transients were also measured on FDB fibres. These calcium transients were visualized using laser scanning confocal microscopy in the line-scan mode. Figure 4 displays representative fluorescence intensity changes during single pulses (panels A and B) and during trains (panels C and D) of depolarizations. Note that the spatial profile of the transients was homogenous in both strains (see expanded images in Fig. 4*A*–*D*), indicating a normal propagation of the depolarization in the T-tubular system.

To analyse the calcium transients, the line-scans were normalized and 10–15 points of the images in the space domain were averaged. Figure 5 presents representative fluorescence transients after normalization using single (top panel) and train (bottom panel) stimulation from control (left) and *Cmpt* (right) mice. Analysis of these transients revealed that the average amplitudes of the calcium transients in *Cmpt* fibres were almost identical during the single stimulation (2.37 ± 0.12 F/F_0, n = 25 in control; 2.50 ± 0.15 F/F_0, n = 26 in *Cmpt*, $P > 0.4$) but significantly reduced during the train stimulation as compared to controls (Table 4).

During the measurements either six or three calcium transients were recorded ~~in~~ for single or train stimulations, respectively. There was no significant decrease in the amplitude of the consecutive transients either in the single (Fig. 5*E*) or in the train (Fig. 5*F*) depolarizations in either animal group.

To further analyse calcium release from the SR, first the normalized fluorescence values of the train depolarisations were transformed to calcium concentration (eqn (2)), and then the total amount of calcium released ($[Ca]_T$) and the calcium release flux (R_{rel}) through the RyRs was calculated (eqns (3)–(5)). It is clear from Fig. 6 that the change in $[Ca^{2+}]_i$ (top panel) as well as the total calcium released into the myoplasm (middle panel), and the corresponding calcium release flux (bottom panel) were reduced in *Cmpt*

mice. R_{rel} reached its peak 9 ms after the onset of the depolarization and was significantly smaller in the *Cmpt* strain (Table 4). Furthermore, a significant difference was observed in the maintained steady level of R_{rel}. On the other hand, the ratio of peak-to-steady level and the time constant of the inactivation remained unchanged, i.e. they were essentially identical in the two animal groups. The amount of released calcium showed roughly a 30% decrease (Table 4) in the mutant animals. The data presented in Figs 4–6 and in Table 4 clearly demonstrate that depolarization-evoked calcium release from the SR was significantly reduced in *Cmpt* mice.

Elementary calcium release events in *Cmpt* fibres. To understand the reasons underlying the suppressed SR calcium release, localized calcium release events were measured in control and in *Cmpt* fibres using high speed laser scanning confocal microscopy. The fibres displayed calcium sparks (calcium release events with large amplitude and short duration) and embers (events with small amplitude and long duration) (Fig. 7*A*). Note that the number of calcium sparks was far greater than that of embers. Although fibres from *Cmpt* mice generated calcium sparks and embers as for control cells (Fig. 7*B*), the characteristic parameters of these events were altered. Plotting the amplitude histograms of sparks (Fig. 8*A*) revealed that the *Cmpt* mutation was associated with an increase in the relative frequency of calcium sparks with smaller amplitudes. Pooled data show that on average the amplitude of the calcium sparks was significantly higher in control fibres than in *Cmpt* cells (0.165 ± 0.001 *vs.* 0.154 ± 0.002, respectively; $P < 0.001$). Similarly, we observed a relatively higher amount of faster evolving sparks in *Cmpt* than in control mice (Fig. 8*B*), the average rise time showed a significant (30%, $P < 0.01$) reduction (from 34.7 ± 0.9 to 24.3 ± 0.8 ms in control and *Cmpt* mice, respectively). Although the overall shape of FWHM histograms remained unaffected in *Cmpt* animals, the distribution was slightly shifted to the left (Fig. 8*C*). That is, the *Cmpt* mutation decreased the average FWHM significantly ($P < 0.01$) from the control 1.92 ± 0.01 to 1.87 ± 0.01 μm. The distribution of event duration was also altered by the mutation (Fig. 8*D*), showing a relatively high frequency of shorter events in *Cmpt*

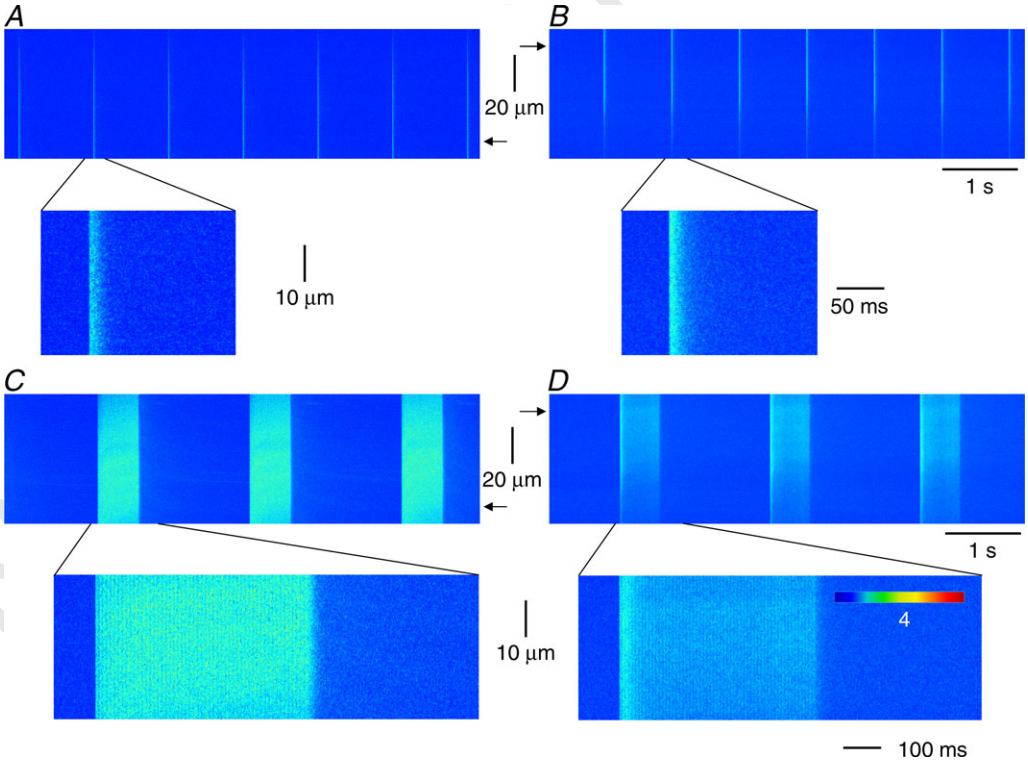

Figure 4. Field stimulation-evoked fluorescence changes in FDB fibres
Intact fibres isolated from the FDB muscles were loaded with the calcium-sensitive fluorescent dye Rhod-2. Suprathreshold pulses were used to initiate action potentials, and the accompanying changes in Rhod-2 fluorescence were detected on a confocal microscope in the line-scan mode. Images of fluorescence intensity changes as evoked by single (*A* and *B*) and trains (*C* and *D*) of depolarizations in control (*A* and *C*) and in *Cmpt* (*B* and *D*) mice. Expanded images in all panels demonstrate the homogenous activation of the fibres. Arrows indicate the spatial point where the time courses presented in Fig. 5 were determined. Acquisition parameters: 4096 × 512 pixels, 1.53 ms line^{-1}, 0.14 μm pixel^{-1}; temperature 22°C.

mice. In addition, and in accordance with the above, the frequency of the spontaneous calcium release events was also significantly ($P < 0.001$) reduced in fibres from *Cmpt* mice (6.2 ± 0.5 Hz) as compared to the control group (33.0 ± 2.7 Hz).

Discussion

Myostatin knock-out as well as *Cmpt* mice – despite their increased muscle weight – were found to have reduced specific force as compared to control animals (Amthor *et al.* 2007). Despite the fact that changes in fibre composition and consequently altered metabolic status of the muscles from these mice have been reported (e.g. Girgenrath *et al.* 2005), a clear explanation for the altered contractile function is not yet available. Here, on the one hand, we complement the observations previously made *in vivo* and, on the other, provide evidence that alterations in calcium signalling but not in the activation of the contractile machinery underlie the reduced force production.

Table 4. Parameters of the depolarization-evoked calcium transients and of the corresponding calcium release flux

	Control ($n = 14$)	*Cmpt* ($n = 13$)[#]
$\Delta F/F_0$	2.42 ± 0.03	2.07 ± 0.10*
$\Delta[Ca^{2+}]_T$ (mM)	3.06 ± 0.39	2.08 ± 0.23*
R_{rel} peak (μM ms^{-1})	23.7 ± 3.0	15.8 ± 2.1*
R_{rel} steady level (μM ms^{-1})	5.7 ± 0.7	3.7 ± 0.5*
R_{rel} peak/steady level	4.3 ± 0.4	4.6 ± 0.6
Time to peak of R_{rel} (ms)	8.9 ± 0.3	8.9 ± 0.2
Tau of inactivation (ms)	6.7 ± 0.9	8.8 ± 1.3

*Significant difference at $P < 0.05$ as compared to control.
[#]Numbers in parentheses denote the number of fibres from three control and three *Cmpt* animals.

Our results from *in vivo* measurements are in agreement with those published earlier for both Mstn$^{-/-}$ (Amthor *et al.* 2007; Savage & McPherron, 2010) and *Cmpt* mice (Amthor *et al.* 2007) showing a reduced physical performance, as *Cmpt* animals were less agile in voluntary

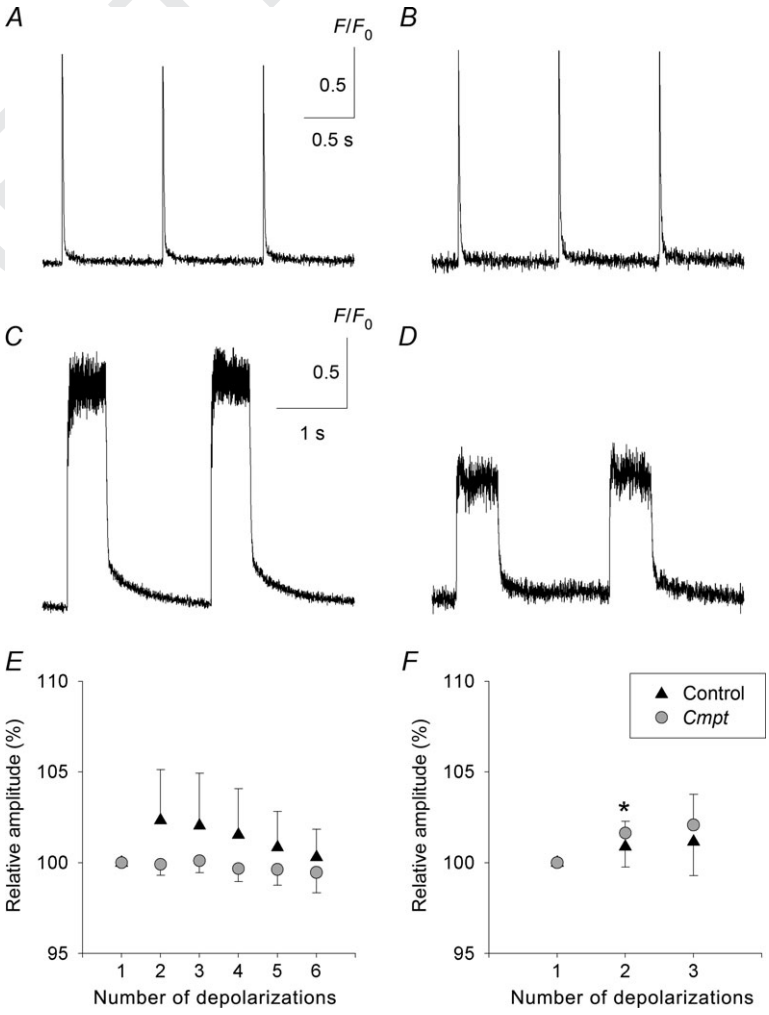

Figure 5. Time course of fluorescence changes in FDB fibres during the depolarisations
The traces (*A–D*) are spatially averaged time courses of Rhod-2 fluorescence of the line-scans in Fig. 4*A–D*, respectively, after normalizing to baseline fluorescence (F/F_0). The average was calculated from 10 consecutive lines of the line-scans at the arrows in Fig. 4. Background was calculated from data points before the depolarization. Average of consecutive peaks of fluorescence intensities normalized to the first peak during the single (*E*) and train (*F*) depolarizations. Pooled data from three control (14 fibres) and three *Cmpt* (13 fibres) animals. *Significant ($P < 0.05$) difference from the first peak.

wheel running. Furthermore, the observation that the normalized force – force normalized to body weight – was reduced in the grip-strength tests in *Cmpt* mice is consistent with the idea that the increased muscle mass was not accompanied by a parallel and proportional increase in overall force. Although it is likely that alterations in cardiovascular and/or respiratory functions also contributed to the reduced physical performance in the activity wheel for these animals, based on previous reports as well as on our own findings mentioned above, changes in the events that couple electrical excitation to contraction are also part of the pathology.

Based on the previously reported changes in fibre metabolism associated with the myostatin mutation, including shifts in the oxidative state of the muscle (Girgenrath *et al.* 2005; Baan *et al.* 2013) as well as a large increase in the ATP cost of contraction (Giannesini *et al.* 2013), it was tempting to assume that an altered acto-myosin interaction would be responsible for the reduced specific force since the former can be accompanied by modifications in myosin expression. In contrast to this expectation we were unable to demonstrate any modification in the p_{Ca} dependence of force production as studied in chemically skinned fibre segments. Neither fast nor slow muscles displayed any change in their p_{Ca}–tension curves. In addition, the maximal attainable tension was also similar in control and *Cmpt* animals.

On the other hand, action potential-evoked calcium transients were significantly reduced in mutant as compared to control animals. This reduction in the increase in $[Ca^{2+}]_i$ during a train of action potentials that is the physiological stimulus during *in vivo* contractions – taken together with the unaltered p_{Ca}–tension relationship – readily explains the reduced overall tension. Note, however, that the reduction in $[Ca^{2+}]_i$ and the

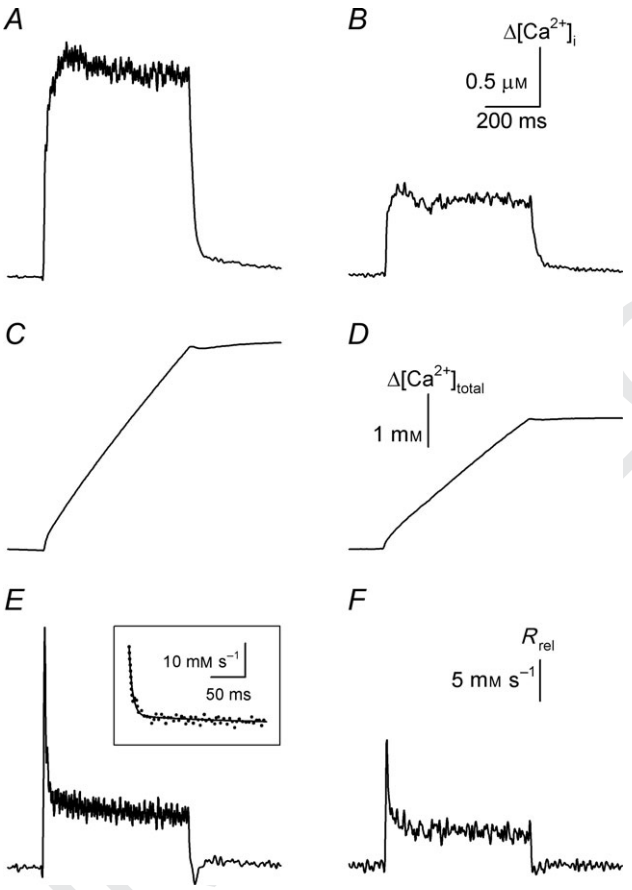

Figure 6. Depolarization-evoked changes in $[Ca^{2+}]_i$ and the corresponding calcium release flux
A and *B*, changes in intracellular calcium concentration calculated from the first transient shown in Fig. 5*C* and *D*, respectively, using eqn (2). *C* and *D*, the amount of calcium released ($[Ca^{2+}]_T$; eqn (3)) from the SR as determined from the transients shown in *A* and *B*. To calculate $[Ca^{2+}]_T$ a removal model – with the following parameters: [dye] = 20 μM, $k_{off,rhod}$ = 130 s^{-1}, $k_{on,rhod}$ = 82 μM^{-1} s^{-1}, [parvalbumin] = 2 mM, Kd_{pump} = 1 μM, $[Ca^{2+}]_{rest}$ = 70 nM – was fitted to the declining phase of the transients following the depolarization (see Methods). *E* and *F*, the corresponding calcium release flux (FL) through the RyRs. The inset in *E* shows an enlarged portion of FL and the fitted exponential (τ = 5.1 ms), which was used to determine the time constant of inactivation.

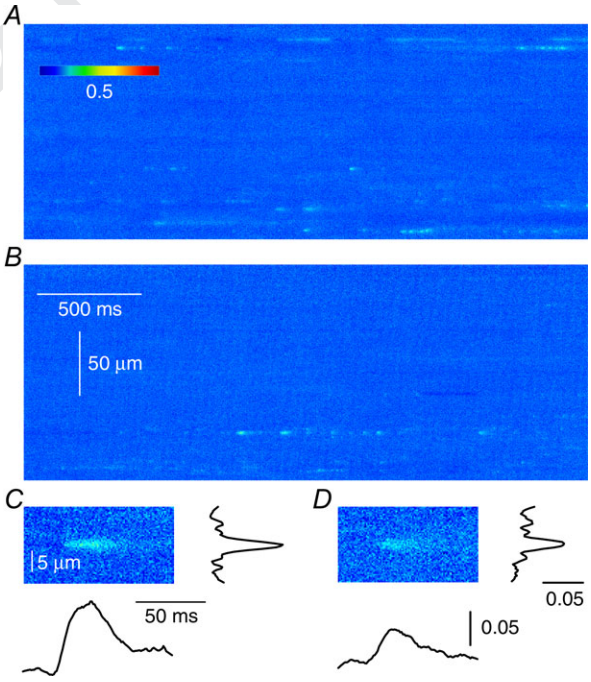

Figure 7. Spontaneous Ca^{2+} release events in FDB fibres
A and *B*, line-scan images from fibres of FDB muscles taken from control (*A*) and from *Cmpt* (*B*) mice. Enzymatically isolated fibres were permeabilized with a brief exposure to 0.01% Saponin and loaded with Fluo-3. *C* and *D*, representative sparks with their spatial profiles and time courses detected in control (*C*) and in *Cmpt* (*D*) mice. Spatial and temporal profiles were calculated from the average of five consecutive rows or columns at the maximum of the event. Acquisition parameters: 4096 × 512 pixels, 1 ms $line^{-1}$, 0.33 μm $pixel^{-1}$; temperature 22°C.

consequently anticipated reduced force, based on the measured p_{Ca}–tension relationship, was proportionally less than the increase in muscle diameter (2.35 ± 0.19 *vs.* 6.93 ± 0.32 mm^2 in the control ($n = 13$) and *Cmpt* ($n = 19$) strains, respectively, for EDL, $P < 0.001$) not accounting fully for the observed greater strength in grip tests.

SR calcium release flux was determined from the global calcium transients and a 33% reduction was observed in both the peak and the maintained steady flux. Since the peak-to-steady ratio was unaltered in *Cmpt* mice, i.e. the waveform of the SR calcium release flux was essentially the same in the mutant and the control animals, the kinetics of activation and inactivation of the calcium release channels was probably not affected. This was further strengthened by the findings that the time-to-peak of SR calcium release flux as well as the rate constant of inactivation, calculated by fitting an exponential function to the declining phase, were essentially unchanged. Note at this point that a slight (but statistically not significant) increase in the time constant was indeed observed, which is in line with previous reports that a reduced SR calcium release would initiate a slower inactivation (see e.g. Sárközi *et al.* 1996). Furthermore, in accordance with the above, a clear reduction in the amount of calcium released from the SR during a train of action potentials was also detected.

These observations leave three possibilities, or their combination, to explain the reported findings. First, there is a reduction in SR calcium content; second, there is a reduction in RyR permeability/conductance; and third, the number of activated RyRs is reduced. It should be stressed, however, that the magnitude of these modifications should not be too extensive or changes in the kinetics of inactivation would accompany the reduced SR calcium release. Indeed, the reduction in SR calcium release flux observed here was within these limits and was comparable to earlier studies in which the effect of SR depletion on the SR calcium release waveform was investigated (Klein *et al.* 1988). Reduced RyR permeability or SR calcium content could be the result of an altered metabolic state of the muscle since the redox sensitivity of RyRs has been demonstrated in a number of publications (e.g. Liu *et al.* 1994; Bull *et al.* 2007; Petrotchenko *et al.* 2011). These reports concluded that reducing conditions transform the channel to a low-open probability state, while oxidative conditions transform it to a high-open probability state (Marengo *et al.* 1998). Therefore, shifts in the redox state of the myoplasm from the control to more reducing would result in a reduced activation, while shifts to a more oxidative state would result in an increased resting SR leak and a consequent reduction in SR calcium content (e.g. Oba *et al.* 2002), both in line with the observations seen here. To determine whether the RyR channels *per se* were affected in the mutant strain, direct measurements of the channel activity would be needed. At present, there are no data available in the literature on RyRs isolated from *Cmpt* or Mstn$^{-/-}$

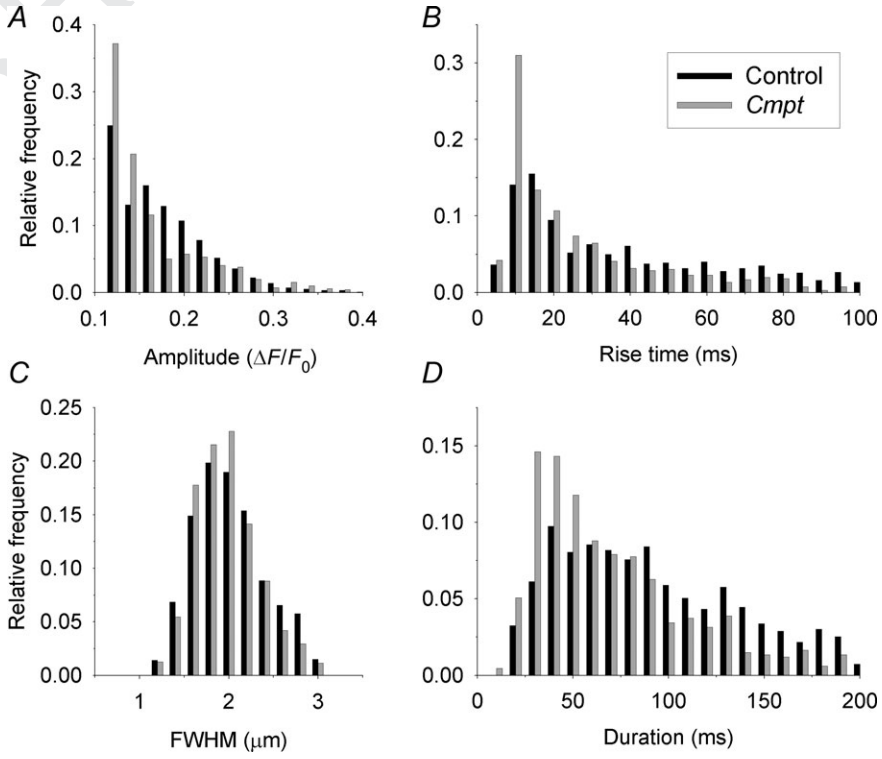

Figure 8. Distribution histograms of calcium release event parameters
Amplitude (*A*), rise time (*B*), FWHM (*C*) and duration (*D*) histograms of calcium release events from control (black bars, eight animals) and from *Cmpt* (grey bars, six animals) mice. Events were identified in the line-scan images with an automated detection routine based on wavelet transformation (see Methods). Values of the selected parameters were binned and plotted as relative frequencies to present their distributions. Events with amplitudes smaller than 0.1 $\Delta F/F_0$ and with FWHM smaller than 0.3 μm were not included in the analysis.

mice. Here we attempted to gain insight into channel function using Saponin-skinned fibres and determining the characteristics of calcium release events. Although these events should be regarded with caution since they do not appear with appreciable frequency in non-skinned fibres, their study appear the only way to tackle channel behaviour in the native environment (Klein & Schneider 2006). Due to the above mentioned clear limitations, only the simplest properties were investigated in detail in this study. It is clear from the results that calcium release events occur with a lower frequency in *Cmpt* animals than they do in control mice (Fig. 7). In addition, these events have a smaller amplitude and FWHM than their control counterparts. These observations are consistent with the idea that channels open less readily and release less calcium once they are opened in the mutant as compared to control mice. Although we cannot exclude the possibility that fibres from *Cmpt* animals respond differently to Saponin treatment, it is more likely that the observed changes are indeed due to alterations in calcium release. This is strengthened by the fact that the observed changes in the parameters of the calcium release events are clearly in line with the alterations seen for global calcium transients in intact fibres. In particular, the reduced number of events and the amount of calcium released per event would readily explain why global calcium transients were smaller in the mutant animals. These findings would then suggest that the alterations that explain the *Cmpt* phenotype – with regard to the reduced force – reside, at least in part, in the calcium release process.

Considering the above, the most likely explanation for the reduced calcium release is a reduction in SR content. This would then influence the release process through at least two routes. The activation of RyRs depends on the calcium concentration inside the SR, namely a lower intraluminar calcium concentration results in a lower activation level of the channels (Laver, 2005). In addition, due to the lower SR calcium, the current through the channels is also reduced. These effects combined would then explain the lower frequency as well as the lower amplitude of the calcium release events and, finally, the reduced calcium transients. Although, at present, we have no clear explanation for how the mutation leads to the reduction in SR calcium content, all the data are consistent with the idea that the reduced specific force of these mice is the consequence of this alteration.

References

Amthor H, Macharia R, Navarrete R, Schuelke M, Brown SC, Otto A, Voit T, Muntoni F, Vrbóva G, Partridge T, Zammit P, Bunger L & Patel K (2007). Lack of myostatin results in excessive muscle growth but impaired force generation. *Proc Natl Acad Sci U S A* **104**, 1835–1840.

Baán JA, Kocsis T, Keller-Pintér A, Müller G, Zádor E, Dux L & Mendler L (2013). The compact mutation of myostatin causes a glycolytic shift in the phenotype of fast skeletal muscles. *J Histochem Cytochem* **61**, 889–900.

Bodine SC, Stitt TN, Gonzalez M, Kline WO, Stover GL, Bauerlein R, Zlotchenko E, Scrimgeour A, Lawrence JC, Glass DJ & Yancopoulos GD (2001). Akt/mTOR pathway is a crucial regulator of skeletal muscle hypertrophy and can prevent muscle atrophy *in vivo*. *Nat Cell Biol* **3**, 1014–1019.

Bull R, Finkelstein JP, Humeres A, Behrens MI & Hidalgo C (2007). Effects of ATP, Mg^{2+}, and redox agents on the Ca^{2+} dependence of RyR channels from rat brain cortex. *Am J Physiol Cell Physiol* **293**, C162–C171.

Bünger L, Laidlaw AH, Bulfield G, Eisen EJ, Medrano JF, Bradford GE, Prichner F, Renne U, Schlote W & Hill WG (2001). Inbred lines of mice derived from long-term on growth selected lines: unique resources for mapping growth genes. *Mamm Genome* **12**, 678–686.

Csernoch L, Kovács L, Nilius B & Szücs G (1990). Caffeine and the myoplasmic calcium removal mechanisms in cut frog skeletal muscle fibres. *Gen Physiol Biophys* **9**, 251–266.

Csernoch L, Pouvreau S, Ronjat M & Jacquemond V (2008). Voltage-activated elementary calcium release events in isolated mouse skeletal muscle fibers. *J Membr Biol* **226**, 43–55.

Elkina Y, von Haehling S, Anker SD & Springer J (2011). The role of myostatin in muscle wasting: an overview. *J Cachexia Sarcopenia Muscle* **2**, 143–151.

Escobar AL, Velez P, Kim AM, Cifuentes F, Fill M & Vergara JL (1997). Kinetic properties of DM-nitrophen and calcium indicators: rapid transient response to flash photolysis. *Pflugers Arch* **434**, 615–631.

Fodor J, Gönczi M, Sztretye M, Dienes B, Oláh T, Szabó L, Csoma E, Szentesi P, Szigeti GP, Marty I & Csernoch L (2008). Altered expression of triadin 95 causes parallel changes in localized Ca^{2+} release events and global Ca^{2+} signals in skeletal muscle cells in culture. *J Physiol* **586**, 5803–5818.

Franzini-Armstrong C & Protasi F (1997). Ryanodine receptors of striated muscles: a complex channel capable of multiple interactions. *Physiol Rev* **77**, 699–729.

Giannesini B, Vilmen C, Amthor H, Bernard M & Bendahan D (2013). Lack of myostatin impairs mechanical performance and ATP cost of contraction in exercising mouse gastrocnemius muscle *in vivo*. *Am J Physiol Endocrinol Metab* **305**, E33–E40.

Girgenrath S, Song K & Whittemore LA (2005). Loss of myostatin expression alters fiber-type distribution and expression of myosin heavy chain isoforms in slow- and fast-type skeletal muscle. *Muscle Nerve* **31**, 34–40.

~~Grobet L, Martin LJ, Poncelet D, Pirottin D, Brouwers B, Riquet J, Schoeberlein A, Dunner S, Ménissier F, Massabanda J, Fries R, Hanset R & Georges M (1997). A deletion in the bovine myostatin gene causes the double-muscled phenotype in cattle. *Nat Genet* **17**, 71–74.~~

~~Hamilton SL & Reid MB (2000). RYR1 modulation by oxidation and calmodulin. *Antioxid Redox Signal* **2**, 41–45.~~

Jacquemond V (2012). Waveless mammalian muscle. *J Physiol* **590**, 1783.

Q2

Q3

Jenes A, Bodnár D, Ruzsnavszky O, Geyer N, Dienes B, Balogh A, Papp Z, Szentesi P & Csernoch L (2012). Modified EC coupling in myostatin deficient ($MSTN^{-/-}$) mice. *J Muscle Res Cell Motil* **33**, 242–243.

Kambadur R, Sharma M, Smith TP & Bass JJ (1997). Mutations in myostatin (GDF8) in double-muscled Belgian Blue and Piedmontese cattle. *Genome Res* **7**, 910–916.

Klein MG, Simon BJ, Szucs G & Schneider MF (1988). Simultaneous recording of calcium transients in skeletal muscle using high- and low-affinity calcium indicators. *Biophys J* **53**, 971–988.

Klein MG & Schneider MF (2006). Ca^{2+} *spark*s in skeletal muscle. *Progr Biophys Mol Biol* **92**, 308–332.

Lai KV, Gonzalez M, Poueymirou WT, Kline WO, Na E, Zlotchenko E, Stitt TN, Economides AN, Yancopoulos GD & Glass DJ (2004). Conditional activation of Akt in adult skeletal muscle induces rapid hypertrophy. *Mol Cell Biol* **24**, 9295–9304.

Lamb G (2002). Voltage-sensor control of Ca^{2+} release in skeletal muscle: insights from skinned fibers. *Front Biosci* **7**, 834–842.

Langley B, Thomas M, Bishop A, Sharma M, Gilmour S & Kambadur R (2002). Myostatin inhibits myoblast differentiation by down-regulating MyoD expression. *J Biol Chem* **277**, 49831–49840.

Laver DR (2005). Coupled calcium release channels and their regulation by luminal and cytosolic ions. *Eur Biophys J* **34**, 359–368.

Liu G, Abramson JJ, Zable AC & Pessah IN (1994). Direct evidence for the existence and functional role of hyperreactive sulfhydryls on the ryanodine receptor-triadin complex selectively labeled by the coumarin maleimide 7-diethylamino-3-(4′-maleimidylphenyl)-4-methylcoumarin. *Mol Pharmacol* **45**, 189–200.

Lukács B, Sztretye M, Almássy J, Sárközi S, Dienes B, Mabrouk K, Simut C, Szabó L, Szentesi P, De Waard M, Ronjat M, Jóna I & Csernoch L (2008). Charged surface area of maurocalcine determines its interaction with the skeletal ryanodine receptor. *Biophys J* **95**, 3497–3509.

Marengo JJ, Hidalgo C & Bull R (1998). Sulfhydryl oxidation modifies the calcium dependence of ryanodine-sensitive calcium channels of excitable cells. *Biophys J* **74**, 1263–1277.

~~Matsakas A, Macharia R, Otto A, Elashry MI, Mouisel E, Romanello V, Sartori R, Amthor H, Sandri M, Narkar V & Patel K (2012). Exercise training attenuates the hypermuscular phenotype and restores skeletal muscle function in the myostatin null mouse. *Exp Physiol* **97**, 125–140.~~

Q4

McPherron AC, Lawler AM & Lee SJ (1997). Regulation of skeletal muscle mass in mice by a new TGF-β superfamily member. *Nature* **387**, 83–90.

Mosher DS, Quignon P, Bustamante CD, Sutter NB, Mellersh CS, Parker HG & Ostrander EA (2007). A mutation in the myostatin gene increases muscle mass and enhances racing performance in heterozygote dogs. *PLoS Genet* **3**, e79.

Oba T, Murayama T & Ogawa Y (2002). Redox states of type 1 ryanodine receptor alter Ca^{2+} release channel response to modulators. *Am J Physiol Cell Physiol* **282**, C684–C692.

Papp Z, Szabo A, Barends JP & Stienen GJM (2002). The mechanism of the force enhancement by Mg-ADP under simulated ischaemic conditions in rat cardiac myocytes. *J Physiol* **543**, 177–189.

Petrotchenko EV, Yamaguchi N, Pasek DA, Borchers CH & Meissner G (2011). Mass spectrometric analysis and mutagenesis predict involvement of multiple cysteines in redox regulation of the skeletal muscle ryanodine receptor ion channel complex. *Res Rep Biol* **2011**, 13–21.

Ríos E & Pizarro G (1991). Voltage sensor of excitation–contraction coupling in skeletal muscle. *Physiol Rev* **71**, 849–908.

Savage KJ & McPherron AC (2010). Endurance exercise training in myostatin null mice. *Muscle Nerve* **42**, 355–362.

Sárközi S, Szentesi P, Jona I & Csernoch L (1996). Effects of cardiac glycosides on excitation–contraction coupling in frog skeletal muscle fibres. *J Physiol* **495**, 611–626.

Schuhmeier RP, Dietze B, Ursu D, Lehmann-Horn F & Melzer W (2003). Voltage-activated calcium signals in myotubes loaded with high concentrations of EGTA. *Biophys J* **84**, 1065–1078.

Szabó G, Dallmann G, Müller G, Patthy L, Soller M & Varga L (1998). A deletion in the myostatin gene causes the compact (*Cmpt*) hypermuscular mutation in mice. *Mamm Genome* **9**, 671–672.

Szabó LZ, Vincze J, Csernoch L & Szentesi P (2010). Improved spark and ember detection using stationary wavelet transforms. *J Theor Biol* **264**, 1279–1292.

Szappanos H, Cseri J, Deli T, Kovács L & Csernoch L (2004). Determination of depolarisation- and agonist-evoked calcium fluxes on skeletal muscle cells in primary culture. *J Biochem Biophys Methods* **59**, 89–101.

Szentesi P, Szappanos H, Szegedi C, Gönczi M, Jona I, Cseri J, Kovács L & Csernoch L (2004). Altered elementary calcium release events and enhanced calcium release by thymol in rat skeletal muscle. *Biophys J* **86**, 1436–1453.

Varga L, Szabó G, Darvasi A, Müller G, Sass M & Soller M (1997). Inheritance and mapping of *Compact* (*Cmpt*), a new mutation causing hypermuscularity in mice. *Genetics* **147**, 755–764.

Varga L, Müller G, Szabó G, Pinke O, Korom E, Kovács B, Patthy L & Soller M (2003). Mapping modifiers affecting muscularity of the myostatin mutant ($Mstn^{Cmpt\text{-}dl1Abc}$) compact mouse. *Genetics* **165**, 257–267.

Additional information

Competing interests

None.

Author contributions

D.B., N.G., O.R., T.O., B.H, M.Sz., J.F., B.D., Á.B., L.Sz. and P.Sz. performed experiments, and collected, analysed and interpreted data. Z.P., G.M., L.Cs. and P.Sz. designed and supervised the study, analysed and interpreted data and wrote the paper.

This work is part of the PhD thesis of D.B. under the supervision of P.Sz. All authors approved the final version of the manuscript. All experiments were performed at the University of Debrecen.

Funding

This work was supported by grants from the Hungarian Scientific Research Found (OTKA NN-107765), from the Hungarian Ministry of Human Resources (TÁMOP-4.2.1/B-09/1/KONV-2010-0007, TÁMOP-4.2.2/B-10/1-2010-0024 and TÁMOP-4.2.2.A-11/1/KONV-2012-0025). This paper was supported by the János Bólyai Research Scholarship of the Hungarian Academy of Sciences to J.F. and the Bridging Fund of UD Faculty of Medicine.

Acknowledgements

None declared.

Queries

Journal: **TJP**
Paper: tjp6059

Dear Author
During the copy-editing of your paper, the following queries arose. Please respond to these by marking up your proofs with the necessary changes/additions. Please write your answers on the query sheet if there is insufficient space on the page proofs. Please write clearly and follow the conventions shown on the corrections sheet. If returning the proof by fax do not write too close to the paper's edge. Please remember that illegible mark-ups may delay publication.

Query No.	Description	Remarks
Q1	Author: please add a footnote defining the parameters in Tables 3 and 4.	
Q2	Autho: Grobet et al 1997 is not cited in text.	
Q3	Author: Hamilton, Reid 2000 is not cited in text.	
Q4	Author: Matsakas et al. 2012 is not cited in text.	

Required software to eAnnotate PDFs: Adobe Acrobat Professional or Acrobat Reader (version 8.0 or above). (Note that this document uses screenshots from Acrobat Reader 9. For screenshots from Acrobat Reader X, a separate document is available on the journal e-proofing site.)
The latest version of Acrobat Reader can be downloaded for free at: http://get.adobe.com/reader/

Once you have Acrobat Reader 8, or higher, open on your PC you should see the Commenting Toolbar:

****(If the above toolbar does not appear automatically go to *Tools>Comment & Markup>Show Comment & Markup Toolbar*)****

1. Replacement Text Tool — For replacing text.

Strikes a line through text and opens up a replacement text box.

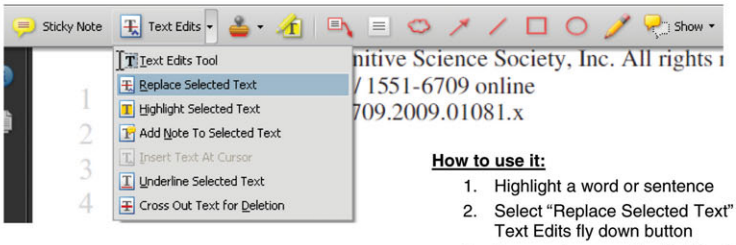

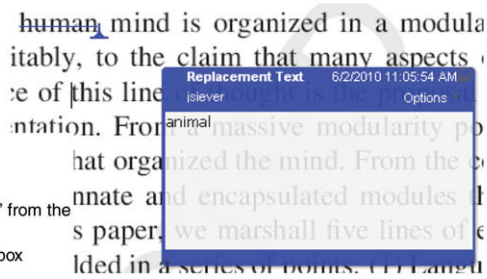

How to use it:

1. Highlight a word or sentence
2. Select "Replace Selected Text" from the Text Edits fly down button
3. Type replacement text in blue box

2. Cross-out Text Tool — For deleting text.

Strikes a red line through selected text.

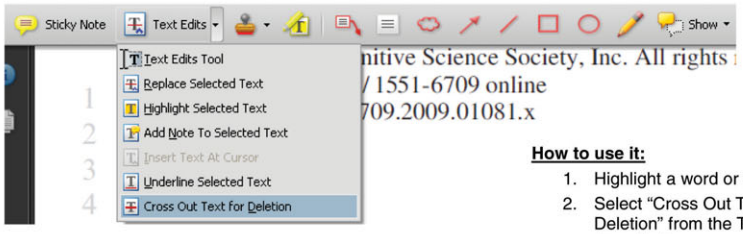

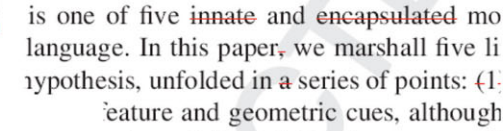

How to use it:

1. Highlight a word or sentence
2. Select "Cross Out Text for Deletion" from the Text Edits fly down button

3. Highlight Tool — For highlighting a selection to be changed to bold or italic.

Highlights text in yellow and opens up a text box.

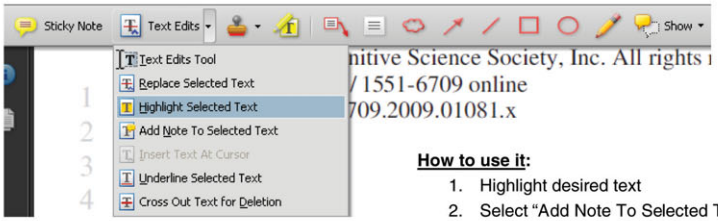

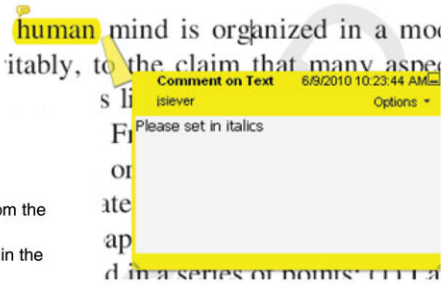

How to use it:

1. Highlight desired text
2. Select "Add Note To Selected Text" from the Text Edits fly down button
3. Type a note detailing required change in the yellow box

4. Note Tool — For making notes at specific points in the text

Marks a point on the paper where a note or question needs to be addressed.

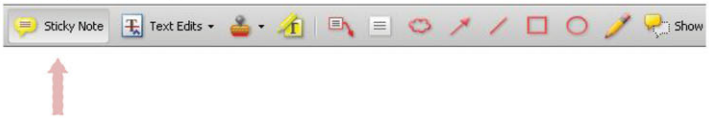

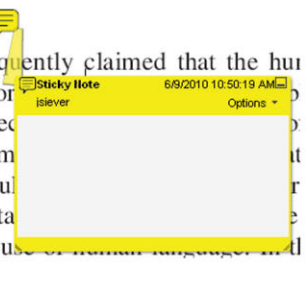

How to use it:

1. Select the Sticky Note icon from the commenting toolbar
2. Click where the yellow speech bubble symbol needs to appear and a yellow text box will appear
3. Type comment into the yellow text box

5. Drawing Markup Tools — For circling parts of figures or spaces that require changes

These tools allow you to draw circles, lines and comment on these marks.

How to use it:

1. Click on one of shape icons in the Commenting Toolbar
2. Draw the selected shape with the cursor
3. Once finished, move the cursor over the shape until an arrowhead appears and double click
4. Type the details of the required change in the red box

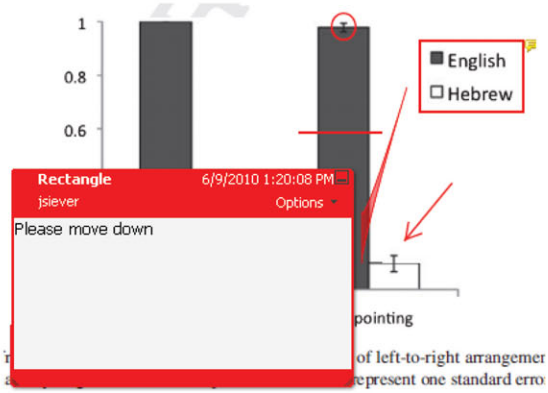

6. Attach File Tool — For inserting large amounts of text or replacement figures as a files.

Inserts symbol and speech bubble where a file has been inserted.

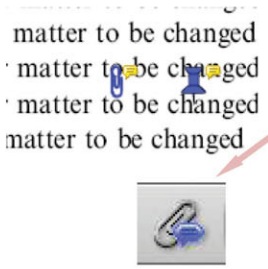

How to use it:

1. Right click on the Commenting Toolbar
2. Select "Attach a File as a Comment"
3. Click on paperclip icon that appears in the Commenting Toolbar
4. Click where you want to insert the attachment
5. Select the saved file from your PC or network
6. Select type of icon to appear (paperclip, graph, attachment or tag) and close

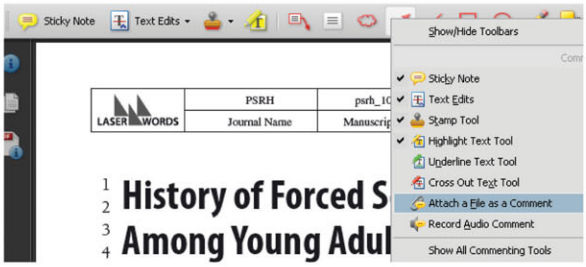

7. Approved Tool (Stamp) — For approving a proof if no corrections are required.

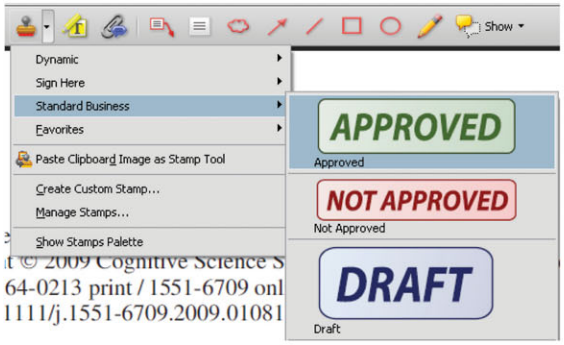

How to use it:

1. Click on the Stamp Tool in the toolbar
2. Select the Approved rubber stamp from the 'standard business' selection
3. Click on the text where you want to rubber stamp to appear (usually first page)

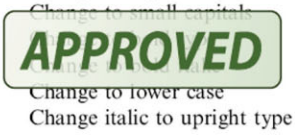

Help

For further information on how to annotate proofs click on the Help button to activate a list of instructions:

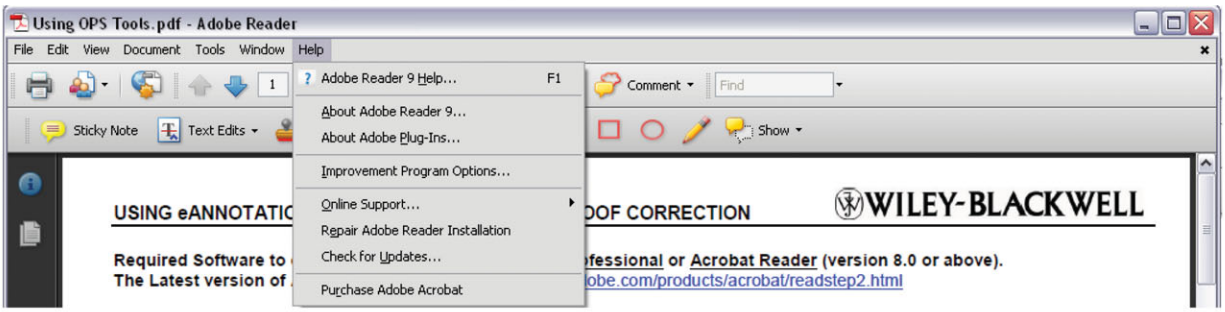

MARKED PROOF

Please correct and return this set

Please use the proof correction marks shown below for all alterations and corrections. If you wish to return your proof by fax you should ensure that all amendments are written clearly in dark ink and are made well within the page margins.

Instruction to printer	*Textual mark*	*Marginal mark*
Leave unchanged	··· under matter to remain	✓
Insert in text the matter indicated in the margin		New matter followed by or
Delete	/ through single character, rule or underline or through all characters to be deleted	 or
Substitute character or substitute part of one or more word(s)	/ through letter or through characters	new character / or new characters /
Change to italics	under matter to be changed	
Change to capitals	under matter to be changed	
Change to small capitals	under matter to be changed	
Change to bold type	under matter to be changed	
Change to bold italic	under matter to be changed	
Change to lower case	Encircle matter to be changed	
Change italic to upright type	(As above)	
Change bold to non-bold type	(As above)	
Insert 'superior' character	/ through character or where required	 or under character e.g.  or 
Insert 'inferior' character	(As above)	 over character e.g. 
Insert full stop	(As above)	⊙
Insert comma	(As above)	,
Insert single quotation marks	(As above)	 or  and/or or
Insert double quotation marks	(As above)	 or  and/or  or 
Insert hyphen	(As above)	
Start new paragraph		
No new paragraph		
Transpose		
Close up	linking  characters	
Insert or substitute space between characters or words	/ through character or where required	
Reduce space between characters or words	between characters or words affected